Available online at BCREC website: https://bcrec.id

Bulletin of Chemical Reaction Engineering & Catalysis, 17 (2) 2022, 420-429

Research Article

H_2O_2 Exfoliation of TiO_2 for Enhanced Hydrogen Production from Photocatalytic Reforming of Methanol

Syaahidah Abdul Razak, Hasliza Bahruji*, Abdul Hanif Mahadi, Hong Wan Yun

Centre for Advanced Materials and Energy Sciences, Universiti Brunei Darussalam, Jalan Tungku Link, Gadong BE1410, Brunei Darussalam.

Received: 22nd March 2022; Revised: 16th May 2022; Accepted: 17th May 2022
Available online: 19th May 2022; Published regularly: June 2022

Abstract

Hydrogen is considered a future energy carrier for clean and sustainable technology. Photocatalytic reforming of methanol produced hydrogen using water and energy from sunlight. This study reported enhanced activity of TiO_2 without metal co-catalyst for hydrogen production following H_2O_2 exfoliation. TiO_2 was transformed into peroxo-titania species on the outer layer of the particles, resulting in surface exfoliation. The exfoliation reduced TiO_2 crystallite sizes enhanced the surface hydroxyl group and reduced the band gap to 3.0 eV. Hydrogen production from methanol-water mixtures on the TiO_2 after four consecutive exfoliations was measured at 300 µmol, significantly higher than the fresh TiO_2 (50 µmol). H_2O_2 exfoliated TiO_2 reduced the pathway for charge migration to the surface. A high concentration of surface hydroxyl group trapped the charge carriers for efficient hydrogen production.

Keywords: H_2O_2; TiO_2; Hydrogen; Methanol; Photocatalyst; Reforming

How to Cite: S.A. Razak, H. Bahruji, A.H. Mahadi, H.W. Yun (2022). H_2O_2 Exfoliation of TiO_2 for Enhanced Hydrogen Production from Photocatalytic Reforming of Methanol. *Bulletin of Chemical Reaction Engineering & Catalysis*, 17(2), 420-429 (doi: 10.9767/bcrec.17.2.13920.420-429)

Permalink/DOI: https://doi.org/10.9767/bcrec.17.2.13920.420-429

1. Introduction

The increase of carbon dioxide levels in the atmosphere from fossil fuels has been a significant threat to the environment. Subsequently, this leads to the development of hydrogen technologies to replace the existing non-renewable source of energy. Hydrogen is considered a future clean energy carrier as no harmful gases are released during combustion [1]. For the long-term treatment of climate change, hydrogen production must satisfy the requirement of being sustainable and pollution-free [2]. Photocatalytic reforming of biofuel is a viable route for hydrogen production under ambient conditions. The reaction occurs through the water splitting process and oxidation of oxygenated organic compounds such as alcohol and sugar [3,4]. In comparison to direct water splitting, photo-reforming process is proven to be more feasible as the undesirable backward reaction between hydrogen and oxygen can be minimized [5,6]. Furthermore, the presence of oxygenated molecules also played the essential role as a sacrificial agent to react with the photogenerated hole and thus, improved the electron and hole pairs lifetime [7,8].

TiO_2 is widely used in many photocatalytic applications due to its low cost, non-toxic and high chemical, and thermal stability [9]. It has a wide bandgap energy of 3.2 eV which can only absorb photons within the UV region for the generation energy carrier in water splitting reaction. The band gap of TiO_2 can be modified to enhance light absorption, for example, by using metal nanoparticles as co-catalysts to enhance

* Corresponding Author.
Email: hasliza.bahruji@ubd.edu.bn (H. Bahruji);

electron-hole separation, anion, or cation doping to reduce band gap [10–13]. Grey TiO_2 nanoparticles produced via aluminium treatment at high temperatures enhanced photocatalytic activity in the visible region by generating oxygen vacancies [14]. In photocatalytic reforming of methanol, TiO_2 is deposited with precious metals, such as Pd, Pt, Au, and Ag, and transition metals, such as Cu and Ni, to provide an electron sink for water reduction [15–17]. The role of metal co-catalysts is also crucial in providing sites for water reduction. Therefore, the absence of metal co-catalysts often results in poor hydrogen generation.

Although TiO_2 showed high photoactivity in UV region, the quantum efficiency was only 0.03 across the UV-AB region, and 0.35 in UV-B region [18]. Surface modification of TiO_2 enhanced quantum efficiency by trapping the photogenerated energy carrier for the generation of highly active hydroxyl species. H_2O_2 is a strong oxidizing reagent based on the formation of OH radicals. H_2O_2 is typically used in advanced oxidation processes (AOPs) to remove dye pollutants due to its solubility in water. A previous study has reported using H_2O_2 in the presence of UV light to decolorize AR88 dye [19]. A band gap narrowing on H_2O_2 modified TiO_2 achieved by in-situ generation of oxygen via thermal decomposition of the peroxo-TiO_2 complex was observed at lower energy, achieving visible light active photocatalytic properties of TiO_2 [20]. Oxygen-richness in TiO_2 photocatalyst treated through facile aqueous peroxo-TiO_2 route enhanced photocatalytic activity to reduce CO_2 to CH_4 [18]. This might be attributed to the excess defects in the catalysts that act as electron scavengers to inhibit recombination reaction between electron-hole pairs and, hence, improve photocatalytic performance. Photocatalytic degradation of RhB dye was also explored using P25 TiO_2 treated with H_2O_2, in which the study exhibited an increase in the degradation rate of nearly 60% under visible light irradiation [19]. Most of the studies on H_2O_2 treated TiO_2 is conducted on photodegradation reaction, in which metal co-catalysts is not required to provide electron sink and sites for water reduction. Most of the studies on H_2O_2 treated TiO_2 is conducted on photodegradation reaction, in which metal co-catalysts is not required to provide electron sink and sites for water reduction. This research aimed to investigate the effect of surface modification on TiO_2 via facile H_2O_2 exfoliation to enhance photocatalytic activity in methanol reforming in the absence of metal co-catalyst. Exfoliation with H_2O_2 was employed to enhance the presence of hydroxyl group on TiO_2 surfaces for efficient electron and hole separation. The photocatalytic activity of the catalysts was determined for hydrogen production from methanol reforming. The changes in structural and optical properties of TiO_2 were studied using X-ray Diffraction (XRD), Fourier Transform Infrared (FTIR), Scanning Electron Microscope - Energy Dispersive X-ray (SEM/EDX), UV-visible and photoluminescence spectroscopy. This study highlighted the ability of TiO_2 to catalyse photocatalytic methanol reforming in the absence of precious metals through surface modification.

2. Materials and Methods

2.1 Catalyst Preparation

A commercial titanium(IV) oxide (TiO_2, Aeroxide P25) powder which contained 80:20 weight ratio of anatase and rutile, respectively, was used throughout the experiment. The exfoliation was carried out by mixing 4 g of commercial TiO_2 with 50 mL 15% wt/wt of hydrogen peroxide (H_2O_2, EMSURE 30%) solution. The mixture was stirred at 40 °C for 4 h. Afterward, the mixture was separated and washed with distilled water at 4000 rev/s for 10 min and dried at 80 °C overnight. The exfoliation was repeated four times by treating the resulting dried solid, keeping the ratio of mass to the total solution of the mixture constant for each treatment. For each treatment, the sample labelled as 'treated TiO_2-n' where n represents the number of exfoliation times.

2.2 Experimental Set-Up

50 mg of catalyst was added to a glass reactor with a rubber stopper and 30 mL of distilled water. The mixture was stirred using a magnetic stirrer for 10 min to ensure efficient dispersion of the solid powder in the solution. Before conducting the test, the solution was first purged with nitrogen gas for 5 minutes to remove air in the glass vial, preventing the backward reaction of hydrogen and oxygen into the water. Once the oxygen in the system was removed, 5 mL of methanol (CH_3OH, EMSURE 99%) was added, and the glass reactor is placed in Opystec Dr Grobel BS-02 irradiation chamber. The interior of irradiation chamber was surrounded by mirrors, employing three MH-lamps of 450 W for UVA-visible light simulation. The wavelength of the UV-visible light was between 350–800 nm. The photocatalytic reaction was carried out continuously for 3 h. The gases that evolved during the reaction were collected and analyzed every 30 min

intervals using gas chromatography GC-2014 Shimadzu with TCD detector.

2.3 Characterization Studies

X-ray Diffraction (XRD, Shimadzu XRD-7000 X-Ray Diffractometer) was employed to determine the crystalline phase of the catalysts powder. The patterns were recorded in the 2θ within a range of 10–60° using a radiation source of λ = 1.54 Å at 40 kV and 30 mA. In addition, the crystallite size of the sample was calculated using the Scherrer equation as shown below:

$$D = \frac{k\lambda}{\beta \cos\theta} \quad (1)$$

where, D is the crystallite size in nm, k is the Scherrer's constant (0.9), λ is the wavelength of X-ray beam (0.15406 nm), θ is the position of the peak in radian, and β is full-width at half-maximum (FWHM) in radian. The surface area of the catalysts is determined by N_2 adsorption (BET surface area, Micromeritics ASAP 2020).

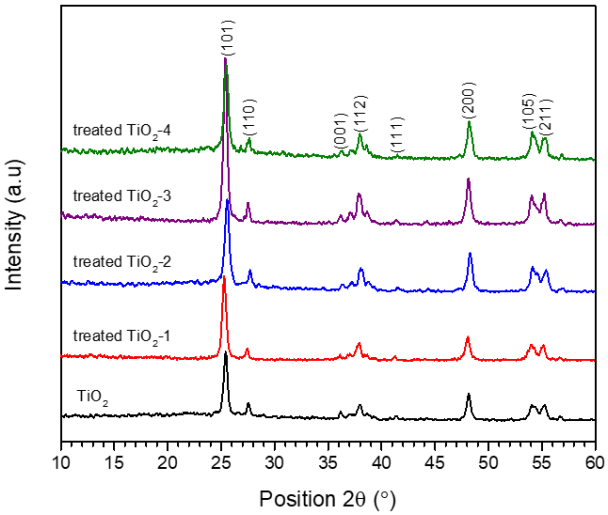

Figure 1. XRD diffraction patterns of treated TiO_2 at exfoliation stages and the commercial TiO_2.

The study of optical absorption properties of the catalysts was carried out using Cary 300 UV-visible spectroscopy. The UV-visible absorption spectra were measured within 200–800 nm. The surface morphology of the samples was studied using JEOL JSM-7610F field emission scanning electron microscope (FESEM) equipped with energy dispersive X-ray spectroscopy (EDX). Fourier-Transform Infrared Spectroscopy (FTIR, Cary 630 FTIR spectrometer) was used to determine the wavelength of light absorbed by the samples and to identify the functional group present that could affect the photocatalytic activity. Photoluminescence (PL) spectra of the samples were obtained using Perkin-Elmer LS-55 spectrophotometer equipped with a pulsed Xenon lamp as an excitation source with a wavelength of 200–900 nm.

3. Results and Discussions

3.1 XRD Analysis

XRD analysis of TiO_2 and exfoliated TiO_2 were shown in Figure 1. The diffraction peaks appeared at 25.4°, 38°, 48.2°, 54°, and 55.3° assigned to the anatase phase of TiO_2, which corresponded to diffraction planes of (101), (112), (200), (105) and (211), respectively. The peaks associated with the rutile phase of TiO_2 were located at 27.6°, 36.2° and 41.4°. There was no significant shift in TiO_2 peaks following treatment with H_2O_2. The crystallite size of TiO_2 was calculated using the Scherrer equation and summarized in Table 1. A reduction in crystallite size of TiO_2 was observed from 14.7 nm to 13.1 nm after treatment with H_2O_2 and did not show any further reduction despite multiple exfoliation stages. Anatase to rutile composition ratios (A) was determined based on the peak intensity of the anatase (101) plane and the rutile (110) plane, as shown in Equation (2).

Table 1. Structural properties of TiO_2 and H_2O_2-treated TiO_2 based on different methods of calculation.

Catalyst	Surface area[a] (m^2/g)	Anatase to rutile ratio[b] (%)	Crystallite size[c] (nm)	Degree of crystallinity[d] (%)	Band gap[e] (eV)	Particle size[f] (nm)
TiO_2	47	75	14.7	45.6	3.23	69
Treated TiO_2-1	50	84	13.1	50.0	3.07	40
Treated TiO_2-2	59	76	13.5	51.2	3.07	N.D
Treated TiO_2-3	52	85	13.5	52.5	3.07	N.D
Treated TiO_2-4	51	77	13.9	51.5	3.08	N.D

[a]Calculated from BET analysis method; [b]Calculated based on Equation (1); [c]Calculated based on Scherrer equation as shown in Equation (2); [d]Calculated based on Equation (3); [e]Calculated based on Tauc plot; [f]Calculated based on particle size distribution from SEM images.

$$A(\%) = \frac{100}{1+1.265\left(\frac{I_R}{I_A}\right)} \quad (2)$$

where, I_R and I_A were the peak intensities of rutile (110) at 27.6° and anatase (101) at 25.4°, respectively.

The degree of crystallinity are presented in Table 1. Following treatment of TiO_2 with H_2O_2, it can be seen that the crystallinity index of TiO_2 has increased from 45.6 to 50.0. However, further exfoliations with H_2O_2 did not show any significant difference on the crystallinity. The degree of crystallinity was calculated using Equation (3).

$$Degree\ of\ crystallinity,\% = \frac{total\ area\ of\ crystalline\ peaks}{total\ area\ of\ crystalline\ and\ amorphous\ peaks} \times 100\% \quad (3)$$

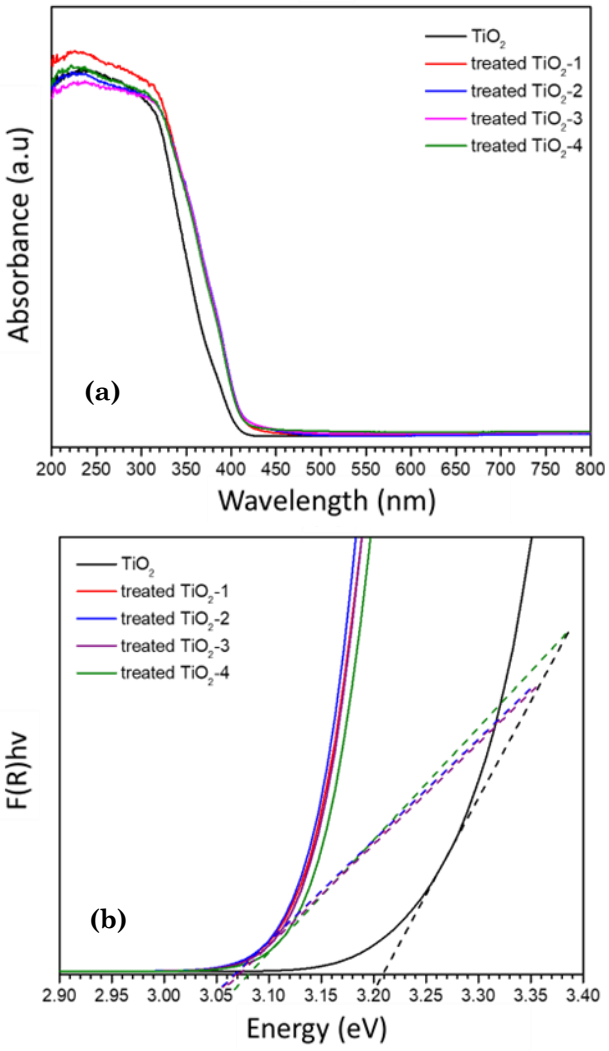

Figure 2. (a) Diffuse Reflectance UV-visible spectra of TiO_2 and treated TiO_2 catalysts (b) Tauc plot for band gap determination for TiO_2 and treated TiO_2 catalysts.

3.2 BET Analysis

BET surface area analysis of the catalysts is shown in Table 1. The surface area of H_2O_2-treated TiO_2 catalysts was increased compared to the fresh TiO_2. TiO_2 was measured at 47 m^2/g, which increased to 50 m^2/g after the first exfoliation. Second exfoliation treatment enhanced the surface area to 59 m^2/g, although the area was reduced with further treatment. It is essential to mention that the TiO_2 was only dried at 80 °C following each exfoliation method. No high-temperature thermal treatment process was conducted during the exfoliation. There was a possibility that treatment with H_2O_2 improved the surface area of TiO_2 by creating a surface defect.

3.3 Diffuse Reflectance UV-visible

Diffuse reflectance UV-visible analysis of the catalysts is displayed in Figure 2(a). All the catalysts showed absorption mainly in the UV region below 400 nm with no significant changes in the absorption properties following treat-

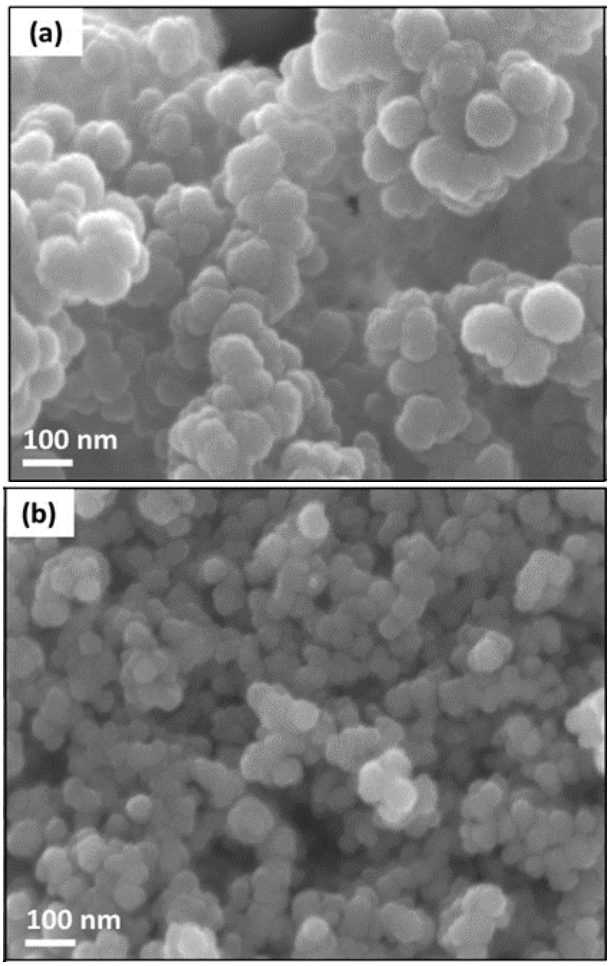

Figure 3. SEM analysis of (a) TiO_2 (b) H_2O_2 treated TiO_2-1.

ment with H_2O_2. The absorption band edge of H_2O_2-treated TiO_2 catalysts around 320–420 nm was shifted slightly towards the visible light region, indicating a change in band gap energy of TiO_2. Tauc plot in Figure 2(b) further verified the reduction of band gap energy of TiO_2 from 3.23 eV to 3.07 eV following treatment with H_2O_2. However, the difference in band gap energy was not significant, in contrast with studies by others that showed H_2O_2 treatment on TiO_2 shifted the band gap energy to the visible region. Ti^{3+} was proposed to increase the absorption of TiO_2 towards visible light [23]. In this case, the result indicated that Ti^{3+} species might only be formed on the surface of TiO_2, which did not change the absorption properties of TiO_2 under the visible light region.

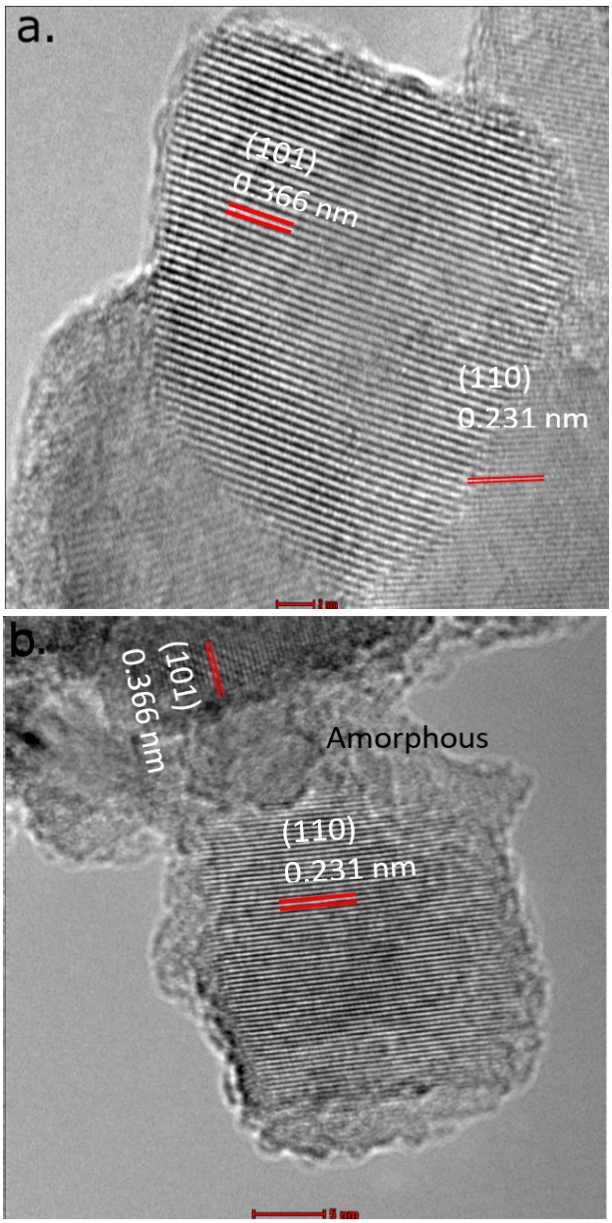

Figure 4. TEM analysis of TiO_2 (a) and H_2O_2 treated TiO_2 -1 (b).

3.4 Morphology Analysis

Figure 3 shows the surface morphology of TiO_2 and H_2O_2-treated TiO_2 after the first exfoliation. Prior to the H_2O_2 treatment, the average particle size of TiO_2 was approximately 69 nm, in which the particles appeared in a uniform spherical shape. TiO_2 nanoparticles also appeared to be agglomerated with other particles to form clusters. Following treatment with H_2O_2, the particle size of TiO_2 was significantly decreased to 40 nm. Nevertheless, TiO_2 nanoparticles retained their spherical shape and remained in cluster form. It is important to note that the calcination process was not employed during the exfoliation, therefore, the reduction of TiO_2 particle size was solely from the exfoliation with H_2O_2.

Figure 4 showed TEM images of TiO_2 and H_2O_2 treated TiO_2 that showed the spherical aggerates of TiO_2 with 10–30 nm size. TiO_2 showed the (101) plane with lattice fringes of 3.66 Å and the parallel (110) planes of the rhombic nanocrystals of the rutile phase with the lattice fringes of 2.31 Å. Rutile (110) and anatase (101) planes were at closed proximity to fresh TiO_2. Following treatment with H_2O_2, amorphous TiO_2 was visibly observed on the perimeter of (101) and (110) crystallites suggesting the exfoliation occurs on the external surface, producing an amorphous TiO_2 layer.

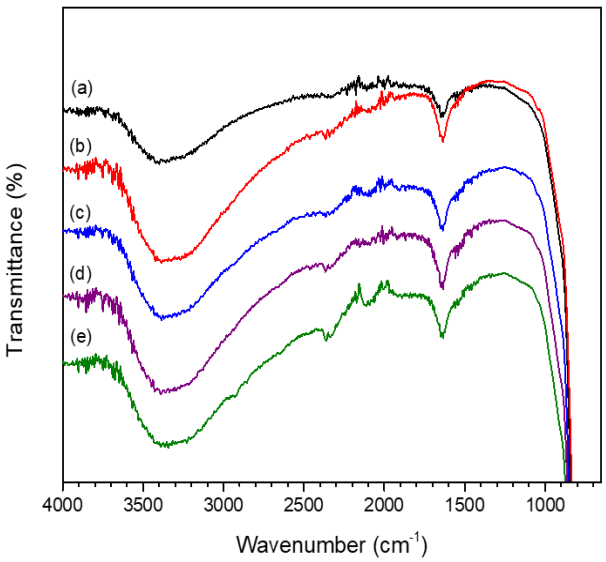

Figure 5. FTIR spectra of (a) TiO_2 (b) treated TiO_2-1 (c) treated TiO_2-2 (d) treated TiO_2-3 (e) treated TiO_2-4.

3.5 FTIR Analysis

FTIR analysis of TiO_2 and H_2O_2-treated TiO_2 catalysts are shown in Figure 5. A strong absorption band cut off at 650 cm^{-1} until 1100 cm^{-1} represented the structure of TiO_2 which is associated with the stretching vibration of Ti–O–Ti bonds [24]. The absorption bands observed at 1643 cm^{-1} and 2400–3700 cm^{-1} corresponded to the hydroxyl group's stretching vibration the surface of TiO_2 due to the presence of adsorbed water [25]. Based on the peak area around 2400–3700 cm^{-1}, the broadening of the hydroxyl band was observed following H_2O_2 treatment on TiO_2. This indicates that the exfoliation via the facile peroxo-titania method created a high surface hydroxyl group on TiO_2.

3.6 Photoluminescence

The photoluminescence (PL) spectroscopy of the catalysts was analyzed to provide evidence of the enhancement of the photogenerated electron-hole pairs' lifetime of TiO_2 following H_2O_2 treatment (Figure 6). The emission intensity of the catalysts was associated with the recombination of the photogenerated electron and hole pairs [26]. Low PL intensity implied reducing the recombination rate of the charge carriers [27]. It can be observed that H_2O_2 treatment on TiO_2 showed a significant reduction of the emission intensity compared to its untreated counterpart.

3.7 Photocatalytic Reforming of Methanol

Figure 7 shows the photocatalytic hydrogen production from methanol using TiO_2 and H_2O_2-treated TiO_2 for 3 h under light irradiation. Untreated TiO_2 underwent an induction period within 60 min before the hydrogen production rate increased steadily at 90 minutes and produced 41 µmol of hydrogen after 180 min. Following treatment with H_2O_2, it can be observed that the photocatalytic activity of treated TiO_2 catalysts was significantly enhanced. The first exfoliation method enhanced the activity of TiO_2 to give ~150 µmol of H_2 in 3h. The induction period is also shorter, in which H_2 started to release at 60 min of reaction. Repeating the exfoliation up to four times further enhanced H_2 yield to 320 µmol in 3h. The overall reaction to the reforming of methanol is shown in Equation (4).

$$CH_3OH + H_2O \rightarrow CO_2 + H_2 \quad (4)$$

The schematic reaction occurs via electron excitation from the conduction band to the valence band of TiO_2 (Equation (5)). The generated hole is trapped by surface hydroxyl radicals generating hydroxyl radicals (Equation (6)). Methanol adsorbed on TiO_2 surface undergoes dehydrogenation catalyzed by hydroxyl radicals generating HCOOH species, subsequently oxidized to form CO_2 (Equations (7) and (8)). The generated H^+ was reduced to produce hydrogen gas (Equation (9)).

Electron excitation on TiO_2:

$$TiO_2 + h\nu \rightarrow h^+ + e^- \quad (5)$$

Hole trapping by surface hydroxyl:

$$h^+ + OH \rightarrow OH^\bullet \quad (6)$$

Methanol dehydrogenation and decomposition:

$$CH_3OH + OH^\bullet \rightarrow HCOOH + 3H^+ \quad (7)$$

$$HCOOH + OH^\bullet \rightarrow CO_2 + H_2O + H^+ \quad (8)$$

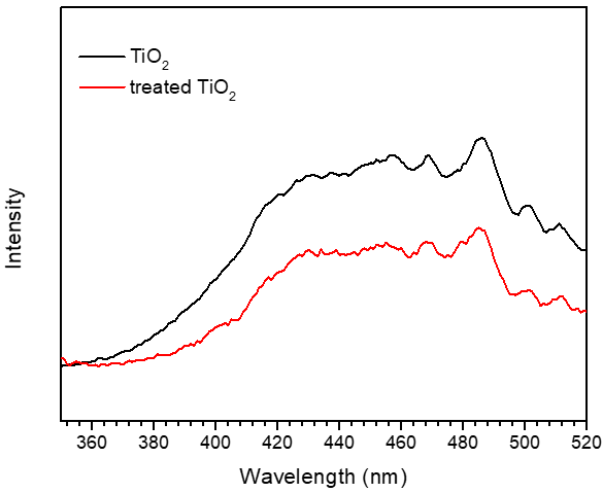

Figure 6. PL spectra of TiO_2 and H_2O_2-treated TiO_2–1.

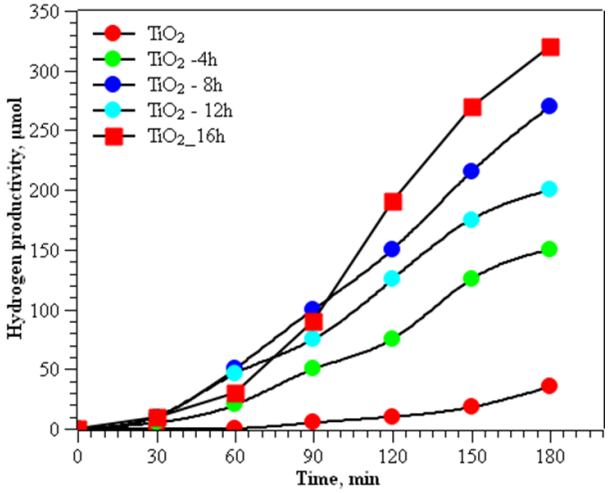

Figure 7. Hydrogen production from methanol using TiO_2 and H_2O_2-treated TiO_2.

Hydrogen generation:

$$4H^+ + 2e^- \rightarrow 2H_2 \quad (9)$$

3.8 Correlation of Structural Properties with Photocatalytic Activity

TiO_2 exfoliation using H_2O_2 significantly enhanced the production of H_2 when using methanol as sacrificial agents. It was reported that H_2O_2 treatment on TiO_2 increased the adsorption in the visible region due to the formation of Ti^{3+} species [28]. HRTEM analysis indicated the closed proximity between (110) rutile crystal plane and (101) anatase crystal plane of TiO_2. Anatase TiO_2 commonly existed as (101) plane, with O termination. Meanwhile, the (110) facet was Ti and O terminated [29]. Theoretical calculation on the surface energy of plane facets indicated the (110) has significantly high surface energy ($E^{110}_{surf} - 0.80$) than the 101 plane ($E^{101}_{surf} - 0.42$) [29]. TiO_2 with different facets have different photoreactivity controlled by their surface atomic structure and surface electronic structure [30]. The hydrogen production from exfoliated TiO_2 was significantly higher than the other studies reported on TiO_2 as summarized in Table 2.

HRTEM analysis of the H_2O_2 treated catalyst showed the appearance of amorphous TiO_2 within the perimeter of the anatase and rutile crystallites. The amorphous structure was also evident by the reduced TiO_2 (101) peak at $2\theta = 25.3°$ and the relative intensity of anatase/rutile following treatment with H_2O_2. Amorphous TiO_2 constituted ~10% of the composition of P25 alongside rutile and anatase that existed separately [38]. Studies on the influence of H_2O_2 sensitized amorphous TiO_2 indicated the formation of peroxide complexes on the amorphous TiO_2 surfaces responsible for adsorption in visible light [39]. Amorphous TiO_2 on its own was inactive for photocatalytic activity due to the recombination sites that existed on the surface defects and the bulk structures [40]. Nevertheless, defects in amorphous TiO_2 that consisted of dangling bonds presumably in the form of Ti−OH showed positive synergy to enhance photoactivity due to the localized Anderson states of amorphous TiO_2 that may increase the photogenerated energy carrier's lifetime [41].

FTIR analysis showed that H_2O_2 treatment increased the density of surface hydroxyl on the TiO_2 surfaces. The high density of surface hydroxyl created Ti−OH dangling bonds, which improved the presence of the surface defect. A high concentration of H_2O_2 produced TiOOH species due to the dissociation of Ti−O−Ti bonds which give the yellow colour powder. The TiOOH was unstable species and released O_2 when heated at 80 °C [42]. The evacuation of

Table 2. Comparison studies of hydrogen production from methanol over commercial and modified TiO_2 photocatalysts.

Photocatalyst	Synthesis Method / Commercial	Light Source	Methanol Concentration	H_2 production	Ref
TiO_2	Treatment with H_2O_2	UVA-visible light source	30 mL of methanol	320 µmol	This study
TiO_2	Hydrothermal	UV lamp: λ = 365 nm	Methanol/water	0.09 mmol	[31]
TiO_2	Sol-gel	Pen-ray Hg lamp: λ = 254 nm λ = 365 nm λ = 450 nm	80% water:20% methanol	252.6 µmol.g^{-1}.h^{-1} 200 µmol.g^{-1}.h^{-1} 0 µmol.g^{-1}.h^{-1}	[32]
TiO_2	Aeroxide P25	UVA-visible light source	30 mL of methanol	41 µmol	This study
TiO_2	Aeroxide P25	300 W Xe lamp	10 v/v%	45 µmol	[33]
TiO_2	Aeroxide P25	300 W Xe lamp	10 v/v%	250 µmol	[34]
TiO_2	Degussa P25	UV light source	5 mL of 50 vol% methanol	6.2 µmol.h^{-1} after 4 cycles	[35]
TiO_2	Degussa P25	15 W black light < 352 nm	30 mL 10v-% methanol	12.5 µmol.g^{-1}	[36]
TiO_2	Degussa P25	300 W Xe lamp	200 mL of 20 vol% methanol	1492 µmol.g^{-1}.h^{-1}	[37]

O_2 resulted in the formation Ti−OH bonds and contributed to the formation of the amorphous layer. This implied that H_2O_2 treatment caused the Ti−O−Ti bond dissociation presumably on the surface of TiO_2 crystallite that contributed to the formation of the amorphous layer. The surface hydroxyl group on TiO_2 suppressed the recombination of energy carriers by trapping the photogenerated holes, as evident by the photoluminescence spectra.

The particle size of the catalyst might also influence the photocatalytic activity of the catalysts. The average particle diameter of the catalysts decreased significantly after treatment with H_2O_2. Rapid transfer of charge carriers occurs in smaller particle sizes attributed to the short distance between two energy levels *i.e.*, valence and conduction bands, and thus, increases the probability of photocatalytic reaction on the TiO_2 surface [43,44]. However, it is essential to note that the rapid recombination rate of electron-hole pairs is also bound to occur when the size of the particle is too small, resulting in the low efficiency of the photocatalytic reaction [45]. Hence, the optimum particle size must be determined to achieve the best photocatalytic activity. On the other hand, having a smaller particle size can also provide a more significant number of active sites for the production of hydrogen [44].

4. Conclusion

Photocatalytic activity of TiO_2 following exfoliation with H_2O_2 for hydrogen production was carried out in photocatalytic reforming of methanol. H_2O_2 treated TiO_2 exhibited a consistent improvement in its catalytic performance and produced a relatively high amount of hydrogen compared to bare TiO_2. Treatment of H_2O_2 on catalysts has changed several parameters of catalysts which believed to be influencing the photocatalytic activity. The combination effects from the reduction in crystallite size, high anatase content, and increased surface hydroxyl group on TiO_2 effectively improved the photocatalytic activity of exfoliated catalysts by inhibiting electron-hole pair recombination rate simultaneously providing more surface-active sites for hydrogen production.

Acknowledgment

The authors would like to acknowledge the University Research Grant for funding this study (UBD/RSCH/1.9/FICBF(b)/2021/011) and the Ministry of Education Brunei Darussalam scholarship to S. Abdul Razak.

References

[1] Nikolaidis, P., Poullikkas, A. (2017). A comparative overview of hydrogen production processes. *Renewable and Sustainable Energy Reviews*, 67, 597–611. DOI: 10.1016/j.rser.2016.09.044.

[2] Kondarides, D.I., Daskalaki, V.M., Patsoura, A., Verykios, X.E. (2008). Hydrogen production by photo-induced reforming of biomass components and derivatives at ambient conditions. *Catalysis Letters*, 122(1–2), 26–32. DOI: 10.1007/s10562-007-9330-3.

[3] Gomathisankar, P., Noda, T., Katsumata, H., Suzuki, T., Kaneco, S. (2014). Enhanced hydrogen production from aqueous methanol solution using TiO_2/Cu as photocatalysts. *Frontiers of Chemical Science and Engineering*, 8(2), 197–202. DOI: 10.1007/s11705-014-1417-y.

[4] Ahmad, H., Kamarudin, S.K., Minggu, L.J., Kassim, M. (2015). Hydrogen from photocatalytic water splitting process: A review. *Renewable and Sustainable Energy Reviews*, 43, 599–610. DOI: 10.1016/j.rser.2014.10.101.

[5] Caravaca, A., Jones, W., Hardacre, C., Bowker, M. (2016). H_2 production by the photocatalytic reforming of cellulose and raw biomass using Ni, Pd, Pt and Au on titania. *Proceedings of the Royal Society A: Mathematical, Physical and Engineering Sciences*, 472(2191) DOI: 10.1098/rspa.2016.0054.

[6] Piras, C.C., Fernández-Prieto, S., De Borggraeve, W.M. (2019). Ball milling: A green technology for the preparation and functionalisation of nanocellulose derivatives. *Nanoscale Advances*, 1(3), 937–947. DOI: 10.1039/c8na00238j.

[7] Ni, M., Leung, M.K.H., Leung, D.Y.C., Sumathy, K. (2007). A review and recent developments in photocatalytic water-splitting using TiO_2 for hydrogen production. *Renewable and Sustainable Energy Reviews*, 11(3), 401–425. DOI: 10.1016/j.rser.2005.01.009.

[8] López, C.R., Melián, E.P., Ortega Méndez, J.A., Santiago, D.E., Doña Rodríguez, J.M., González Díaz, O. (2015). Comparative study of alcohols as sacrificial agents in H_2 production by heterogeneous photocatalysis using Pt/TiO_2 catalysts. *Journal of Photochemistry and Photobiology A: Chemistry*, 312, 45–54. DOI: 10.1016/j.jphotochem.2015.07.005.

[9] De Oliveira Melo, M., Silva, L.A. (2011). Photocatalytic production of hydrogen: An innovative use for biomass derivatives. *Journal of the Brazilian Chemical Society*, 22(8), 1399–1406. DOI: 10.1590/S0103-50532011000800002.

[10] Wu, B.H., Liu, W.T., Chen, T.Y., Perng, T.P., Huang, J.H., Chen, L.J. (2016). Plasmon-enhanced photocatalytic hydrogen production on Au/TiO_2 hybrid nanocrystal arrays. *Nano Energy*, 27, 412–419. DOI: 10.1016/j.nanoen.2016.07.029.

[11] Wen, M., Mori, K., Kuwahara, Y., Yamashita, H. (2017). Plasmonic Au@Pd Nanoparticles Supported on a Basic Metal–Organic Framework: Synergic Boosting of H_2 Production from Formic Acid. *ACS Energy Letters*, 2(1), 1–7. DOI: 10.1021/acsenergylett.6b00558.

[12] Langhammer, C., Yuan, Z., Zorić, I., Kasemo, B. (2006). Plasmonic properties of supported Pt and Pd nanostructures. *Nano Letters*, 6(4), 833–838. DOI: 10.1021/nl060219x.

[13] Mahmoud, M.A. (2014). Plasmon resonance hybridization of gold nanospheres and palladium nanoshells combined in a rattle structure. *Journal of Physical Chemistry Letters*, 5(15), 2594–2600. DOI: 10.1021/jz501201p.

[14] Ariyanti, D., Dong, J., Dong, J., Gao, W. (2016). Visible Light Photocatalytic Properties of Modified Titanium Dioxide Nanoparticles via Aluminium Treatment. *Bulletin of Chemical Reaction Engineering & Catalysis*, 11(1), 40–46. DOI: 10.9767/BCREC.11.1.414.40-46.

[15] Tian, H., Zhang, X.L., Scott, J., Ng, C., Amal, R. (2014). TiO_2 -supported copper nanoparticles prepared via ion exchange for photocatalytic hydrogen production. *Journal of Materials Chemistry A*, 2(18), 6432–6438. DOI: 10.1039/C3TA15254E.

[16] Bahruji, H., Bowker, M., Davies, P.R., Kennedy, J., Morgan, D.J. (2015). The importance of metal reducibility for the photoreforming of methanol on transition metal-TiO_2 photocatalysts and the use of non-precious metals. *International Journal of Hydrogen Energy*, 40(3), 1465–1471. DOI: 10.1016/j.ijhydene.2014.11.097.

[17] Montoya, A.T., Gillan, E.G. (2018). Enhanced Photocatalytic Hydrogen Evolution from Transition-Metal Surface-Modified TiO_2. *ACS Omega*, 3(3), 2947–2955. DOI: 10.1021/acsomega.7b02021.

[18] Bahruji, H., Maarof, H., Abdul Rahman, N. (2019). Quantum efficiency of Pd/TiO_2 catalyst for photocatalytic reforming of methanol in ultra violet region. *Chemical Papers*, 73(11), 2707–2714. DOI: 10.1007/S11696-019-00822-W.

[19] Modirshahla, N., Behnajady, M.A., Rahbarfam, R., Hassani, A. (2012). Effects of Operational Parameters on Decolorization of C. I. Acid Red 88 by UV/H_2O_2 Process: Evaluation of Electrical Energy Consumption. *CLEAN – Soil, Air, Water*, 40(3), 298–302. DOI: 10.1002/CLEN.201000574.

[20] Etacheri, V., Seery, M.K., Hinder, S.J., Pillai, S.C. (2011). Oxygen rich titania: A dopant free, high temperature stable, and visible-light active anatase photocatalyst. *Advanced Functional Materials*, 21(19), 3744–3752. DOI: 10.1002/adfm.201100301.

[21] Tan, L.L., Ong, W.J., Chai, S.P., Mohamed, A.R. (2014). Band gap engineered, oxygen-rich TiO_2 for visible light induced photocatalytic reduction of CO_2. *Chemical Communications*, 50(52), 6923–6926. DOI: 10.1039/c4cc01304b.

[22] Kang, S., Zhang, L., Liu, C., Huang, L., Shi, H., Cui, L. (2017). Hydrogen peroxide activated commercial P25 TiO_2 as efficient visible-light-driven photocatalyst on dye degradation. *International Journal of Electrochemical Science*, 12(6), 5284–5293. DOI: 10.20964/2017.06.54.

[23] Wen, P., Zhang, Y., Xu, G., Ma, D., Qiu, P., Zhao, X. (2019). Ti^{3+} self-doped TiO_2 as a photocatalyst for cyclohexane oxidation under visible light irradiation. *Journal of Materiomics*, 5(4), 696–701. DOI: 10.1016/J.JMAT.2019.04.009.

[24] Ayodhya, D., Perka, S., Nambigari, N. (2018). Sunlight-driven efficient photocatalytic and antimicrobial studies of microwave-assisted Ir-doped TiO_2 nanoparticles for environmental safety. *Nanochemistry Research*, 3(1), 36–49. DOI: 10.22036/NCR.2018.01.005.

[25] Eghbali, P., Hassani, A., Sündü, B., Metin, Ö. (2019). Strontium titanate nanocubes assembled on mesoporous graphitic carbon nitride ($SrTiO_3$/mpg-C_3N_4): Preparation, characterization and catalytic performance. *Journal of Molecular Liquids*, 290, 111208. DOI: 10.1016/J.MOLLIQ.2019.111208.

[26] Li, Q., Anpo, M., Wang, X. (2020). Application of photoluminescence spectroscopy to elucidate photocatalytic reactions at the molecular level. *Research on Chemical Intermediates 2020 46:10*, 46(10), 4325–4344. DOI: 10.1007/S11164-020-04209-5.

[27] Li, H., Zhang, W., Liu, Y. (2020). HZSM-5 zeolite supported boron-doped TiO_2 for photocatalytic degradation of ofloxacin. *Journal of Materials Research and Technology*, 9(2), 2557–2567. DOI: 10.1016/J.JMRT.2019.12.086.

[28] Wu, C.Y., Tu, K.J., Lo, Y.S., Pang, Y.L., Wu, C.H. (2016). Alkaline hydrogen peroxide treatment for TiO_2 nanoparticles with superior water-dispersibility and visible-light photocatalytic activity. *Materials Chemistry and Physics*, 181, 82–89. DOI: 10.1016/J.MATCHEMPHYS.2016.06.036.

[29] Andrés, J., Gracia, L., Gouveia, A.F., Ferrer, M.M., Longo, E. (2015). Effects of surface stability on the morphological transformation of metals and metal oxides as investigated by first-principles calculations. *Nanotechnology*, 26(40) DOI: 10.1088/0957-4484/26/40/405703.

[30] Pan, J., Liu, G., Lu, G.Q., Cheng, H.M. (2011). On the True Photoreactivity Order of {001}, {010}, and {101} Facets of Anatase TiO_2 Crystals. *Angewandte Chemie International Edition*, 50(9), 2133–2137. DOI: 10.1002/ANIE.201006057.

[31] Im, Y., Kang, S., Kim, K.M., Ju, T., Han, G.B., Park, N.K., Lee, T.J., Kang, M. (2013). Dynamic hydrogen production from methanol/water photo-splitting using core@shell-structured CuS@TiO_2 catalyst wrapped by high concentrated TiO_2 Particles. *International Journal of Photoenergy*, 2013 DOI: 10.1155/2013/452542.

[32] Camposeco, R., Hinojosa-Reyes, M., Zanella, R. (2021). Highly efficient photocatalytic hydrogen evolution by using Rh as co-catalyst in the Cu/TiO_2 system. *International Journal of Hydrogen Energy*, 46(51), 26074–26086. DOI: 10.1016/J.IJHYDENE.2021.01.216.

[33] Jung, M., Ng, Y.H., Jiang, Y., Scott, J., Amal, R. (2013). Active Cu Species in Cu/TiO_2 for Photocatalytic Hydrogen Evolution. Chemeca 2013: Challenging Tomorrow.

[34] Jung, M., Scott, J., Ng, Y.H., Jiang, Y., Amal, R. (2014). Impact of Cu oxidation state on photocatalytic H_2 production by Cu/TiO_2. *Proceedings of the 2014 International Conference on Nanoscience and Nanotechnology, ICONN 2014*, 4–6. DOI: 10.1109/ICONN.2014.6965246.

[35] Montoya, A.T., Gillan, E.G. (2018). Enhanced Photocatalytic Hydrogen Evolution from Transition-Metal Surface-Modified TiO_2. *ACS Omega*, 3(3), 2947–2955. DOI: 10.1021/ACSOMEGA.7B02021.

[36] Gomathisankar, P., Noda, T., Katsumata, H., Suzuki, T., Kaneco, S. (2014). Enhanced hydrogen production from aqueous methanol solution using TiO_2/Cu as photocatalysts. *Frontiers of Chemical Science and Engineering* 8(2), 197–202. DOI: 10.1007/S11705-014-1417-Y.

[37] Xu, Q., Ma, Y., Zhang, J., Wang, X., Feng, Z., Li, C. (2011). Enhancing hydrogen production activity and suppressing CO formation from photocatalytic biomass reforming on Pt/TiO_2 by optimizing anatase–rutile phase structure. *Journal of Catalysis*, 278(2), 329–335. DOI: 10.1016/J.JCAT.2011.01.001.

[38] Ohno, T., Sarukawa, K., Tokieda, K., Matsumura, M. (2001). Morphology of a TiO_2 Photocatalyst (Degussa, P-25) Consisting of Anatase and Rutile Crystalline Phases. *Journal of Catalysis*, 203(1), 82–86. DOI: 10.1006/JCAT.2001.3316.

[39] Zou, J., Gao, J., Xie, F. (2010). An amorphous TiO_2 sol sensitized with H_2O_2 with the enhancement of photocatalytic activity. *Journal of Alloys and Compounds*, 497(1–2), 420–427. DOI: 10.1016/J.JALLCOM.2010.03.093.

[40] Ohtani, B., Ogawa, Y., Nishimoto, S. (1997). Photocatalytic Activity of Amorphous−Anatase Mixture of Titanium(IV) Oxide Particles Suspended in Aqueous Solutions. *The Journal of Physical Chemistry B*, 101(19), 3746–3752. DOI: 10.1021/jp962702+.

[41] Bickley, R.I., Gonzalez-Carreno, T., Lees, J.S., Palmisano, L., Tilley, R.J.D. (1991). A structural investigation of titanium dioxide photocatalysts. *Journal of Solid State Chemistry*, 92(1), 178–190. DOI: 10.1016/0022-4596(91)90255-G.

[42] Boonstra, A.H., Mutsaers, C.A.H.A. (1975). Adsorption of hydrogen peroxide on the surface of titanium dioxide. *The Journal of Physical Chemistry*, 79(18), 1940–1943. DOI: 10.1021/J100585A011.

[43] Bahruji, H., Bowker, M., Davies, P.R. (2019). Influence of TiO_2 structural properties on photocatalytic hydrogen gas production. *Journal of Chemical Sciences*, 131(4), 33. DOI: 10.1007/S12039-019-1608-7.

[44] Li, D., Song, H., Meng, X., Shen, T., Sun, J., Han, W., Wang, X. (2020). Effects of particle size on the structure and photocatalytic performance by alkali-treated TiO_2. *Nanomaterials*, 10(3), 1–14. DOI: 10.3390/nano10030546.

[45] Topcu, S., Jodhani, G., Gouma, P.I. (2016). Optimized nanostructured TiO_2 photocatalysts. *Frontiers in Materials*, 3, 1–9. DOI: 10.3389/fmats.2016.00035.